Supporting Information

New high T_c multiferroics $KBiFe_2O_5$ with narrow band gap and promising photovoltaic effect

Ganghua Zhang[1,2], Hui Wu[3,4], Guobao Li[1], Qingzhen Huang[3], Chongyin Yang[2], Fuqiang Huang[1,2] *, Fuhui Liao[1] & Jianhua Lin[1] *

[1]State Key Laboratory of Rare Earth Materials Chemistry and Applications, College of Chemistry and Molecular Engineering, Peking University, Beijing 100871 (P.R. China); [2]CAS Key Laboratory of Materials for Energy Conversion, Shanghai Institute of Ceramics, Chinese Academy of Sciences, Shanghai 200050 (P.R. China); [3]NIST Center for Neutron Research, National Institute of Standards and Technology, Gaithersburg, MD 20899-6102 (USA); [4]Department of Materials Science and Engineering, University of Maryland, College Park, MD 20742 (USA).

Table S1. Typical ferroelectric oxides.

Compound	structure	T_c (K)	E_g (eV)	Efficiency limit (%)
$BiFeO_3$	perovskite	1376	2.67[1]	7
$BaTiO_3$	perovskite	408	3.28[2]	2
$PbTiO_3$	perovskite	763	3.18[3]	2.5
$LiNbO_3$	perovskite	1373	3.78[4]	0.5
$LuFe_2O_4$	spinel	350[5]	2.18[5]	19
CrV_2O_4	spinel	33[6]	--	--
$CoCr_2O_4$	spinel	25[7]	3.1[8]	3
$FeCr_2O_4$	spinel	140[9]	2.9[10]	5
$KBiFe_2O_5$	$A_2B_2O_5$	780	1.6	30

References:

1. Basu, S.R., Martin, L.W., Chu, Y.H., Gajek, M., Ramesh, R., Rai, R.C., Xu, X., Musfeldt, J.L. Photoconductivity in $BiFeO_3$ thin films. *Appl. Phys. Lett.* **92,** 091905 (2008).
2. Wemple, S.H. Polarization fluctuations and the optical-absorption edge in $BaTiO_3$. *Phys. Rev. B* **2,** 2679-2689 (1970).
3. Lazaro, S.de, Longo, E., Sambrano, J.R., Beltrán, A. Structural and electronic properties of $PbTiO_3$ slabs: a DFT periodic study. *Surf. Sci.* **552,** 149–159 (2004).
4. Redfield, D., Burke, W.J. Optical absorption edge of $LiNbO_3$. *J. Appl. Phys.* **45,** 4566-4571 (1974).
5. Rai, R.C., Delmont, A., Sprow, A., Cai, B., Nakarm, M.L. Spin-charge-orbital coupling in multiferroic $LuFe_2O_4$ thin films. *Appl. Phys. Lett.* **100,** 212904 (2012).
6. Giovannetti, G., Stroppa, A., Picozzi, S., Baldomir, D., Pardo, V., Blanco-Canosa, S., Rivadulla, F., Jodlauk, S., Niermann, D., Rohrkamp, J., Lorenz, T., Streltsov, S., Khomskii, D.I., Hemberger, J. Dielectric properties and magnetostriction of the collinear multiferroic spinel CdV_2O_4. *Phys. Rev. B* **83,** 060402(R) (2011).
7. Yamasaki, Y., Miyasaka, S., Kaneko, Y., He, J.-P., Arima, T., Tokura, Y. Magnetic Reversal of the ferroelectric polarization in a multiferroic spinel oxide. *Phys. Rev. Lett.* **96,** 207204 (2006).
8. Suchomski, C., Reitz, C., Brezesinski, K., de Sousa, C.T., Rohnke, M., Iimura, K., de Araujo, J.P.E., Brezesinski, T. Structural, optical, and magnetic properties of highly ordered mesoporous MCr_2O_4 and $MCr_{2-x}Fe_xO_4$ (M = Co, Zn) spinel thin films with uniform 15 nm diameter pores and tunable nanocrystalline domain sizes. *Chem. Mater.* **24,** 155−165 (2012).
9. Singh, K., Maignan, A., Simon, C., Martin. C. $FeCr_2O_4$ and $CoCr_2O_4$ spinels: Multiferroicity in the collinear magnetic state? *Appl. Phys. Lett.* **99,** 172903 (2011).
10. Sudesh, T.L., Wijesinghe, L., Blackwood, D.J. Characterisation of passive films on 300 series stainless steels. *App. Surf. Sci.* **253,** 1006 (2006).

Table S2. Crystal data and structure refinement parameters for $KBiFe_2O_5$

Empirical formula	$KBiFe_2O_5$
FW	439.78
T (K)	296(2)
λ (Å)	0.71073
Space group	$P2_1cn$
a (Å)	7.9841(5)
b (Å)	11.8192(8)
c (Å)	5.7393(4)
$\alpha=\beta=\gamma$ (deg)	90
V (Å^3)	541.59(6)
Z	4
D_{calc} (g/cm^3)	5.394
μ (mm^{-1})	38.400
Goodness-of-fit on F^2	1.000
R_1, wR_2 [$I>2\theta(I)$]	0.0229, 0.0569
R_1, wR_2 [all data]	0.0285, 0.0607

Table S3. Structural parameters of $KBiFe_2O_5$ single crystal at room temperature[a].

Atom	*x*	*y*	*z*	*g*	U_{iso}(×100Å^2)
Bi	0.0231(3)	0.334742(18)	0.24945(17)	1	0.618(11)
K	1.0103(9)	0.86449(18)	0.2476(9)	1	1.04(6)
Fe1	0.23872(18)	0.5890(3)	0.2751(4)	1	0.495(17)
Fe2	0.30603(18)	0.4112(4)	0.7757(4)	1	0.495(17)
O1	1.018(3)	0.6412(5)	0.251(3)	1	0.76(8)
O2	0.307(2)	0.5292(12)	0.9835(13)	1	1.3(2)
O3	0.238(2)	0.4753(12)	0.5073(13)	1	0.8(2)
O4	0.1768(18)	0.2940(10)	0.915(2)	1	0.8(3)
O5	0.3746(19)	0.7060(10)	0.408(2)	1	0.8(3)
Selected bond lengths (Å)					
Bi-O5$^{\#1}$	2.130(13)	Bi-O2$^{\#4}$	2.712(16)	Fe2-O3	1.801(11)
Bi-O4$^{\#2}$	2.174(13)	Fe1-O1$^{\#5}$	1.873(19)	Fe2-O1$^{\#4}$	1.807(19)
Bi-O4$^{\#3}$	2.329(12)	Fe1-O3	1.893(12)	Fe2-O2	1.836(12)
Bi-O5$^{\#4}$	2.345(13)	Fe1-O2$^{\#3}$	1.896(10)	Fe2-O4	1.902(13)
Bi-O3	2.809(10)	Fe1-O5	1.916(13)		

[a] Space group $P2_1cn$ (No. 33); Z=4; a = 7.9841(5) Å, b = 11.8192(8) Å, c = 5.7393(4) Å, V= 541.59(6) Å^3. g = occupation factor.

Symmetry transformations were used to generate equivalent atoms:

#1 x-1/2, y-1/2, -z+1/2; #2 x, -y+1/2, z-1/2; #3 x, y, z-1;

#4 x-1/2, 1-y, 1-z ; #5 x-1, y, z.

Table S4. Refined structural parameters of $KBiFe_2O_5$ from NPD data at 5K: Nuclear space group $P2_1cn$, No. 33, a = 7.99117(6) Å, b = 11.7858(1) Å, c = 5.72967(4) Å, V=539.639(9).

Atom	Site	Occup.	x	y	z	U_{iso} (x100Å^2)
Fe1	*4a*	1.0	0.2076(4)	0.5910(2)	0.2787(4)	0.14(1)
Fe2	*4a*	1.0	0.2751(4)	0.0878(2)	0.2702(4)	0.14(1)
Bi	*4a*	1.0	0.5	0.83512(8)	0.2494(7)	0.18(2)
K	*4a*	1.0	-0.004(1)	0.8681(1)	0.255(1)	0.38(5)
O1	*4a*	1.0	0.2799(8)	0.5280(7)	-0.0075(8)	0.50(2)
O2	*4a*	1.0	0.2120(8)	0.0272(7)	-0.0046(9)	0.50(2)
O3	*4a*	1.0	0.3461(7)	0.7062(6)	0.4058(7)	0.30(2)
O4	*4a*	1.0	0.1487(7)	0.2056(6)	0.4188(7)	0.30(2)
O5	*4a*	1.0	-0.0066(7)	0.6422(1)	0.2391(8)	0.30(3)
Bond lengths						
Fe1-O1	1.891(7)		Bi-O1	2.762(7)	K-O2	2.954(10)
Fe1-O2	1.866(8)		Bi-O2	2.734(7)	K-O2	2.955(10)
Fe1-O3	1.898(7)		Bi-O3	2.149(7)	K-O3	3.495(11)
Fe1-O5	1.830(6)		Bi-O3	2.372(7)	K-O3	3.554(12)
Fe2-O1	1.868(8)		Bi-O4	2.292(6)	K-O4	3.453(11)
Fe2-O2	1.802(7)		Bi-O4	2.161(7)	K-O4	3.516(11)
Fe2-O4	1.917(7)		K-O1	2.914(11)	K-O5	2.6634(28)
Fe2-O5	1.859(6)		K-O1	2.934(11)	K-O5	2.963(10)
					K-O5	2.772(10)
Bond angles						
O1-Fe1-O2	106.1(5)		O1-Fe2-O2	108.1(5)	O3-Bi-O3	84.51(21)
O1-Fe1-O3	115.82(27)		O1-Fe2-O4	103.76(30)	O3-Bi-O4	78.62(23)
O1-Fe1-O5	107.94(25)		O1-Fe2-O5	104.64(24)	O3-Bi-O4	90.11(7)
O2-Fe1-O3	105.56(30)		O2-Fe2-O4	121.88(28)	O3-Bi-O4	156.01(8)
O2-Fe1-O5	110.30(24)		O2-Fe2-O5	111.99(25)	O3-Bi-O4	76.66(21)
O3-Fe1-O5	110.93(29)		O4-Fe2-O5	104.91(28)	O4-Bi-O4	86.37(21)

Table S5. Refined structural parameters of $KBiFe_2O_5$ from NPD data at 300K: Nuclear space group $P2_1cn$, No. 33, a = 7.98557(8) Å, b = 11.8225(1) Å, c = 5.73960(5) Å, V=541.87(1).

Atom	Site	Occup.	x	y	z	U_{iso} (x100Å^2)
Fe1	*4a*	1.0	0.2064(6)	0.5908(3)	0.2765(7)	0.17(1)
Fe2	*4a*	1.0	0.2738(7)	0.0878(3)	0.2722(7)	0.17(1)
Bi	*4a*	1.0	0.5	0.8348(1)	0.2490(9)	0.43(3)
K	*4a*	1.0	-0.016(1)	0.8676(2)	0.250(2)	0.52(7)
O1	*4a*	1.0	0.275(1)	0.5287(8)	-0.006(1)	0.85(3)
O2	*4a*	1.0	0.209(1)	0.0263(8)	-0.004(1)	0.85(3)
O3	*4a*	1.0	0.339(1)	0.7101(6)	0.405(1)	0.64(3)
O4	*4a*	1.0	0.143(1)	0.2027(6)	0.418(1)	0.64(3)
O5	*4a*	1.0	-0.007(1)	0.6422(1)	0.236(1)	0.53(4)
Bond lengths						
Fe1-O1	1.868(9)		Bi-O1	2.788(10)	K-O2	2.987(12)
Fe1-O2	1.870(11)		Bi-O2	2.729(10)	K-O2	2.892(13)
Fe1-O3	1.918(8)		Bi-O3	2.148(8)	K-O3	3.516(11)
Fe1-O5	1.828(8)		Bi-O3	2.408(8)	K-O3	3.589(13)
Fe2-O1	1.873(11)		Bi-O4	2.268(8)	K-O4	3.416(13)
Fe2-O2	1.823(10)		Bi-O4	2.162(8)	K-O4	3.483(11)
Fe2-O4	1.908(8)		K-O1	2.982(13)	K-O5	2.668(4)
Fe2-O5	1.861(8)		K-O1	2.919(12)	K-O5	2.954(14)
					K-O5	2.794(14)
Bond angles						
O1-Fe1-O2	106.8(6)		O1-Fe2-O2	107.5(6)	O3-Bi-O3	82.84(24)
O1-Fe1-O3	117.4(4)		O1-Fe2-O4	103.3(4)	O3-Bi-O4	79.26(29)
O1-Fe1-O5	107.46(34)		O1-Fe2-O5	105.3(4)	O3-Bi-O4	90.33(12)
O2-Fe1-O3	106.2(4)		O2-Fe2-O4	120.9(4)	O3-Bi-O4	155.86(12)
O2-Fe1-O5	109.9(4)		O2-Fe2-O5	112.26(35)	O3-Bi-O4	75.92(25)
O3-Fe1-O5	108.88(35)		O4-Fe2-O5	106.20(34)	O4-Bi-O4	88.06(24)

Table S6. Refined structural parameters of $KBiFe_2O_5$ from NPD data at 698K: Space group $P2_1cn$, No. 33 (nuclear), a = 7.9974(1) Å, b = 11.9168(2) Å, c = 5.7690(1) Å, V=549.81(2).

Atom	Site	Occup.	x	y	z	U_{iso} (x100Å^2)
Fe1	*4a*	1.0	0.210(1)	0.5888(6)	0.2711(9)	1.88(3)
Fe2	*4a*	1.0	0.276(1)	0.0879(6)	0.2768(9)	1.88(3)
Bi	*4a*	1.0	0.5	0.8337(2)	0.244(1)	2.71(6)
K	*4a*	1.0	-0.021(2)	0.8663(5)	0.246(3)	4.4(2)
O1	*4a*	1.0	0.282(1)	0.525(1)	0.005(1)	3.65(7)
O2	*4a*	1.0	0.214(1)	0.029(1)	-0.013(1)	3.65(7)
O3	*4a*	1.0	0.334(1)	0.7115(8)	0.409(1)	3.44(8)
O4	*4a*	1.0	0.140(1)	0.1997(8)	0.414(1)	3.44(8)
O5	*4a*	1.0	-0.003(1)	0.6401(2)	0.230(1)	2.9(1)
Bond lengths						
Fe1-O1	1.806(11)		Bi-O1	2.852(14)	K-O2	3.100(19)
Fe1-O2	1.884(13)		Bi-O2	2.712(14)	K-O2	2.792(21)
Fe1-O3	1.938(13)		Bi-O3	2.187(13)	K-O3	3.519(19)
Fe1-O5	1.830(12)		Bi-O3	2.405(13)	K-O3	2.571(22)
Fe2-O1	1.885(12)		Bi-O4	2.301(13)	K-O4	3.425(22)
Fe2-O2	1.878(11)		Bi-O4	2.158(13)	K-O4	3.479(18)
Fe2-O4	1.894(13)		K-O1	3.133(21)	K-O5	2.6634(28)
Fe2-O5	1.869(12)		K-O1	2.842(19)	K-O5	2.983(25)
					K-O5	2.796(25)
Bond angles						
O1-Fe1-O2	103.8(7)		O1-Fe2-O2	111.6(7)	O3-Bi-O3	82.3(4)
O1-Fe1-O3	120.3(6)		O1-Fe2-O4	102.9(6)	O3-Bi-O4	79.0(4)
O1-Fe1-O5	109.2(6)		O1-Fe2-O5	103.3(5)	O3-Bi-O4	90.47(21)
O2-Fe1-O3	106.7(6)		O2-Fe2-O4	118.8(6)	O3-Bi-O4	156.55(21)
O2-Fe1-O5	110.6(6)		O2-Fe2-O5	110.6(6)	O3-Bi-O4	77.3(4)
O3-Fe1-O5	106.2(5)		O4-Fe2-O5	108.4(5)	O4-Bi-O4	88.9(4)

Table S7. Refined structural parameters of $KBiFe_2O_5$ from NPD data at 863 K: Space group *P*2/*c*, No. 13, *a* = 7.8987(1) Å, *b* = 6.0331(1) Å, *c* = 5.7744(1) Å, V=274.39(1).

Atom	Site	Occup.	x	y	z	U_{iso} (x100Å^2)
Fe	*4g*	1.0	0.2282(1)	0.1635(2)	0.2625(2)	2.64(3)
Bi	*2f*	1.0	0.5	0.6724(3)	0.25	3.10(6)
K	*2e*	1.0	0	0.685(1)	0.25	5.1(1)
O1	*4g*	1.0	0.7188(3)	0.0666(4)	0.5289(5)	4.71(7)
O2	*4g*	1.0	0.6567(3)	0.4151(4)	0.1064(4)	4.52(7)
O3	*2e*	1.0	0	0.2273(5)	0.25	4.7(1)

Bond lengths				Bond angles	
Fe-O1	1.8587(31)	K-O2 ×2	3.5782(28)	O1-Fe-O1	107.19(9)
Fe-O1	1.8652(31)	K-O3 ×2	2.9342(13)	O1-Fe-O2	105.15(14)
Fe-O2	1.8966(31)	K-O3	2.767(7)	O1-Fe-O2	118.64(14)
Fe-O3	1.8396(16)	K-O3	3.266(7)	O1-Fe-O3	108.47(12)
Bi-O1 ×2	2.7255(31)			O1-Fe-O3	110.62(14)
Bi-O2 ×2	2.3801(27)			O2-Fe-O3	106.66(14)
Bi-O2 ×2	2.1873(30)			O3-Bi-O3 ×2	84.13(9)
K-O1 ×2	3.653(5)			O3-Bi-O3	89.58(16)
K-O1 ×2	2.891(4)			O3-Bi-O3 ×2	77.70(11)
K-O2 ×2	3.220(4)			O3-Bi-O3	154.33(18)

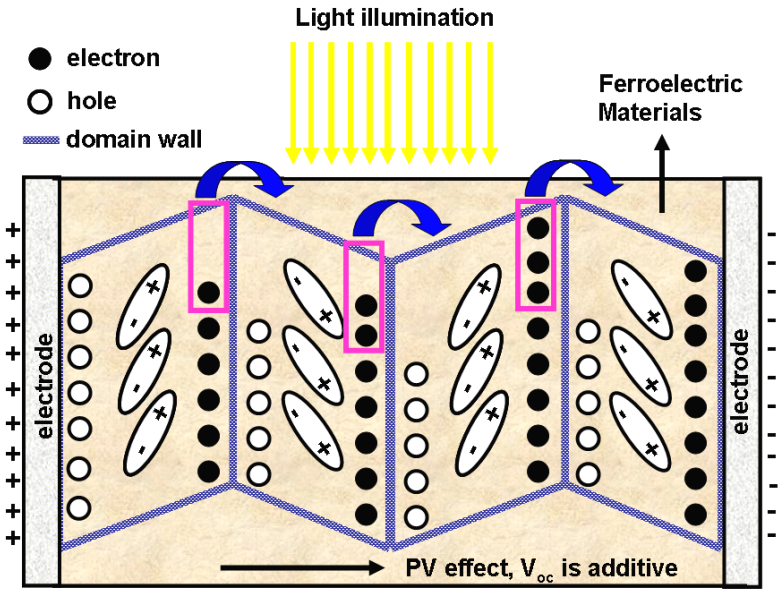

Figure S1. Schematic illustration of physical mechanism of photovoltaic effect driven by multi-domains in ferroelectric materials.

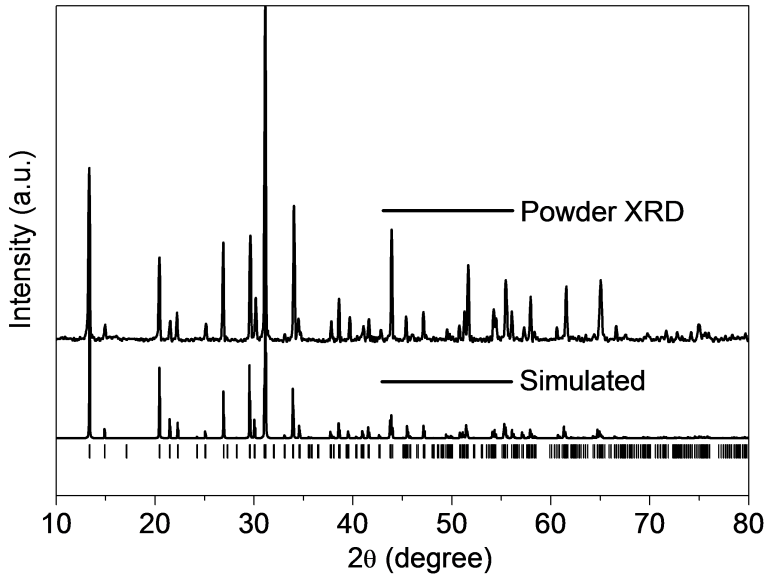

Figure S2. Powder XRD pattern and the simulated XRD pattern for $KBiFe_2O_5$.

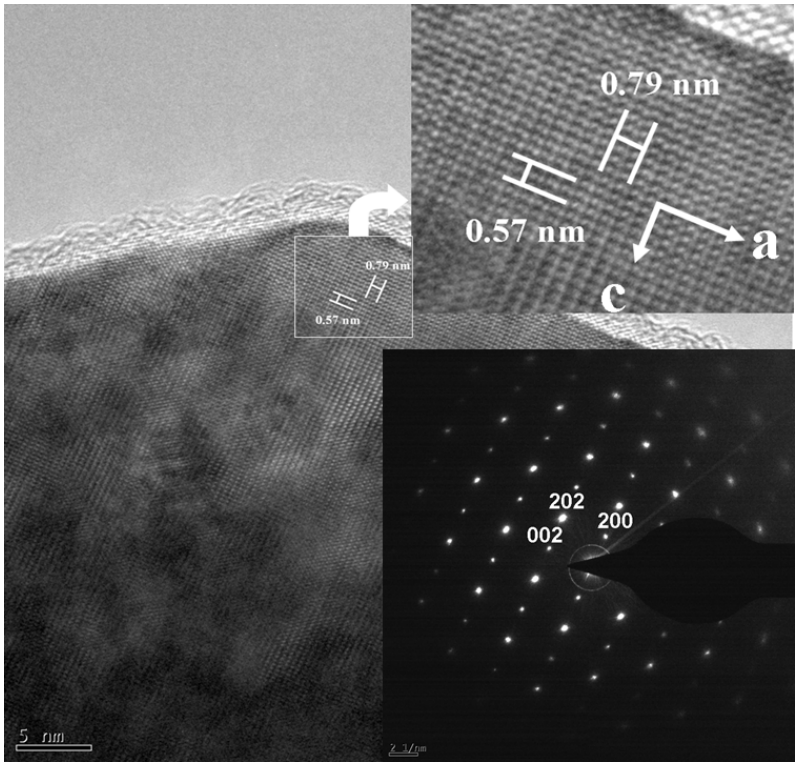

Figure S3. High resolution TEM image at room temperature along the [010] direction. Inset: enlarged view of image (top) and electron diffraction pattern along [010] zone axis (bottom).

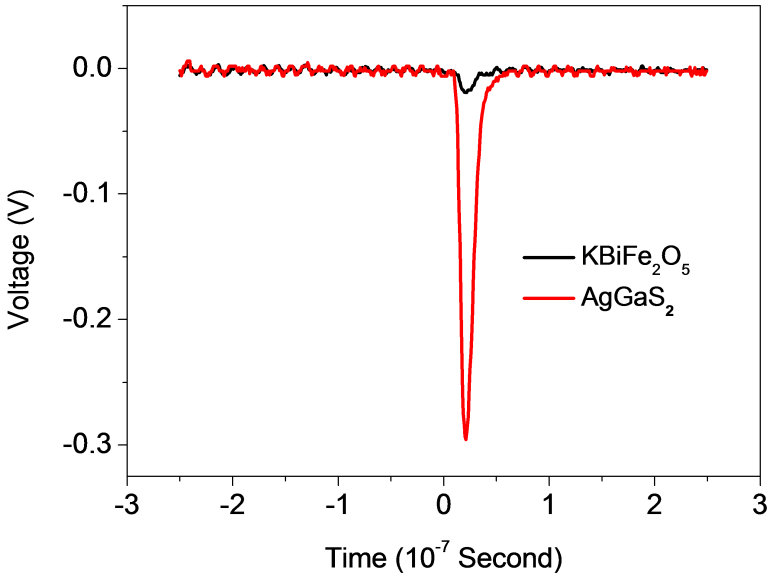

Figure S4. Nonlinear optical second-harmonic generation (SHG) excited by *Q*-switched Nd:YAG l064 nm laser, generating green light of 532nm having about 10% of SHG intensity of $AgGaS_2$.

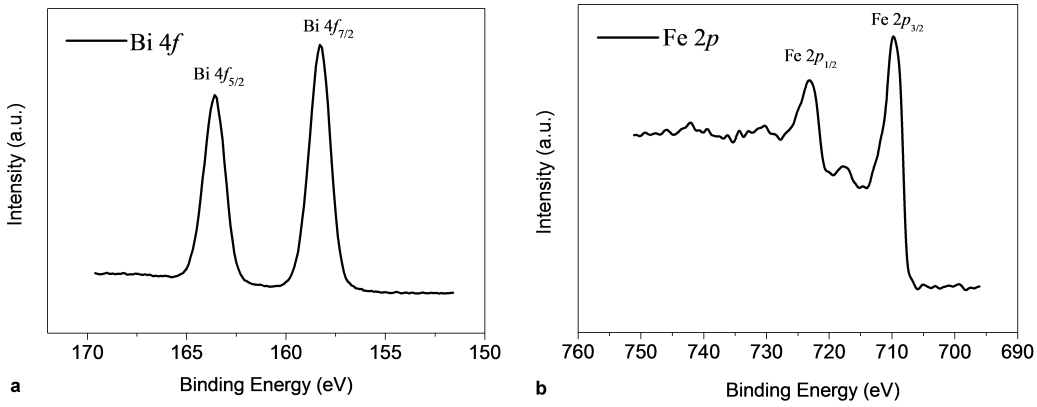

Figure S5. XPS spectrum of $KBiFe_2O_5$: (a) Bi 4*f* and (b) Fe 2*p*.

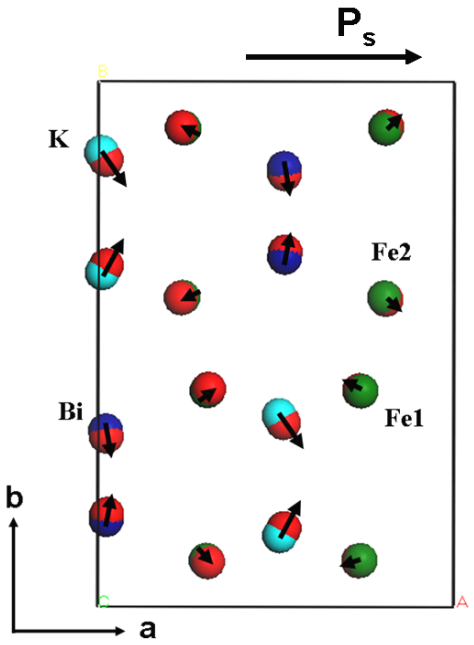

Figure S6. Schematic ion locations and their associated dipole moments (red balls for the center-of-mass positions of coordinating oxygens around each cation). Total ionic contribution (P_s ~ 1.47 μC/cm^2 along the positive *a*-axis) is obtained by summing dipole moments of cations in a unit cell assuming nominal charge for ions.

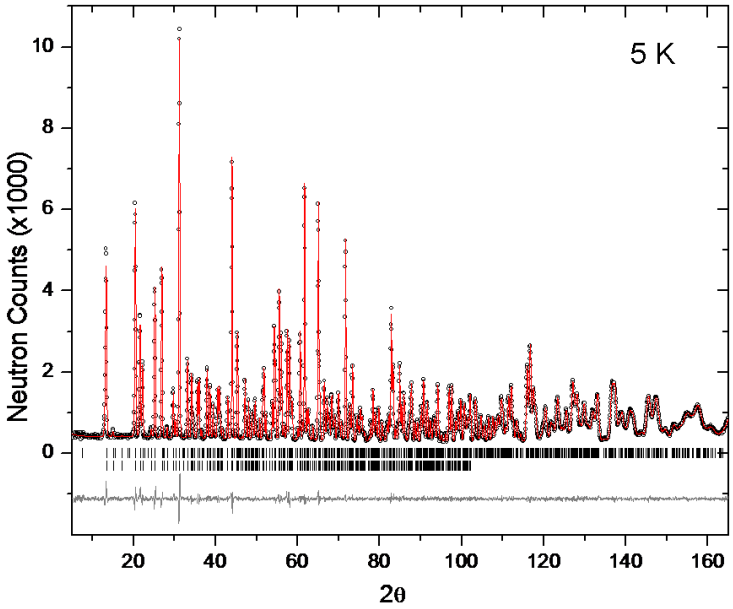

Figure S7. Experimental (circles), calculated (line), and difference (noisy line below observed and calculated patterns) NPD profiles for $KBiFe_2O_5$ at 5K. Vertical bars indicate calculated positions of Bragg peaks from the nuclear phase (upper) and from the magnetic phase (lower). λ=1.5403Å. Space group $P2_1cn$, No. 33, a = 7.99117(6) Å, b = 11.7858(1) Å, c = 5.72967(4) Å, V=539.639(9) Å^3; R_{wp}=0.0331, R_p=0.0278, χ^2=1.159. Magnetic symmetry of Shubnikov group: $P2_1'cn'$ with Fe moment of 3.87(2) μ_B along c-axis direction.

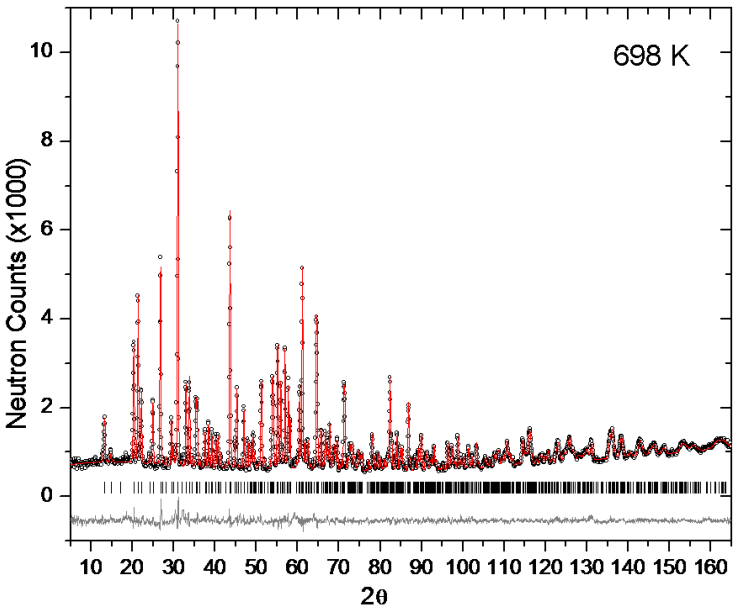

Figure S8. Experimental (circles), calculated (line), and difference (noisy line below observed and calculated patterns) NPD profiles for $KBiFe_2O_5$ at 698 K. Vertical bars indicate calculated positions of Bragg peaks from the nuclear phase. λ=1.5403Å. Space group $P2_1cn$, No. 33, a = 7.9974(1) Å, b = 11.9168(2) Å, c = 5.7690(1) Å, V=549.81(2) Å^3; R_{wp}=0.0436, R_p=0.0350, χ^2=2.019.

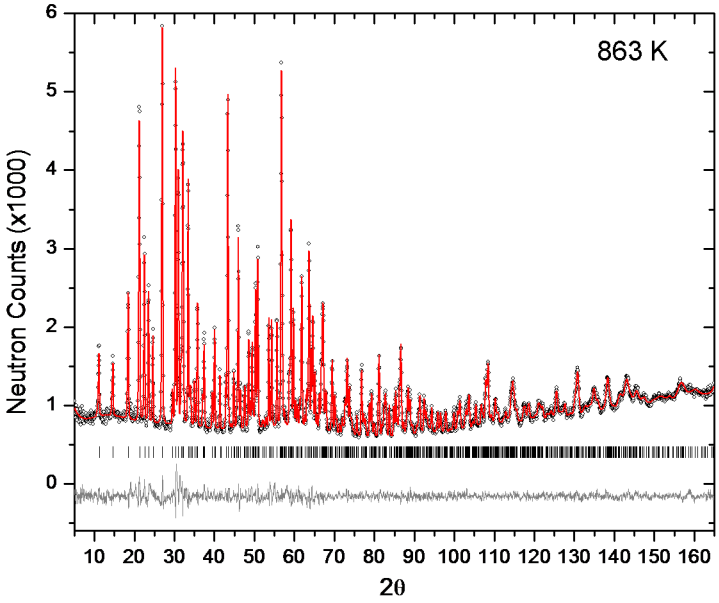

Figure S9. Experimental (circles), calculated (line), and difference (noisy line below observed and calculated patterns) NPD profiles for $KBiFe_2O_5$ at 863 K. Vertical bars indicate calculated positions of Bragg peaks. λ=1.5403Å. Space group *P*2/*c*, No. 13, *a* = 7.8987(1) Å, *b* = 6.0331(1) Å, *c* = 5.7744(1) Å, *V*=274.39(1) Å^3; R_{wp}=0.0389, R_p=0.0312, χ^2=1.690.

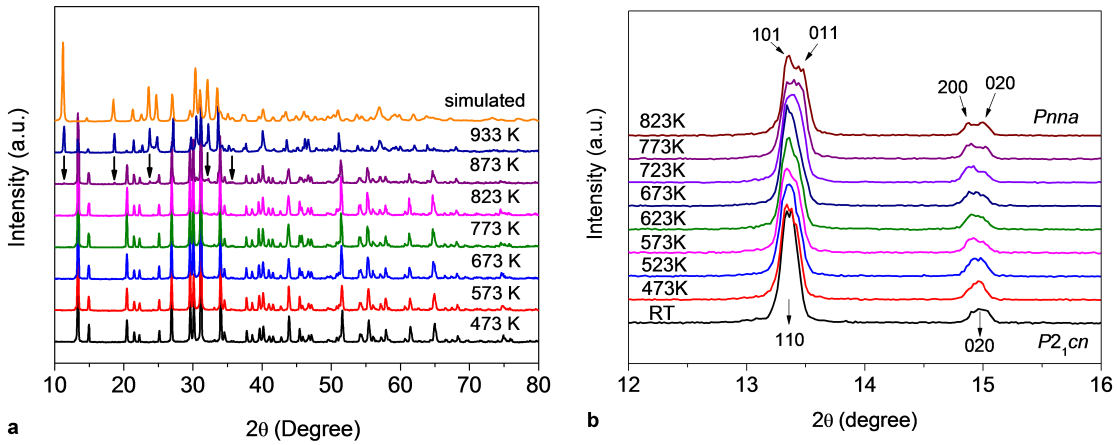

Figure S10. (a) Temperature-dependent XRD patterns for $KBiFe_2O_5$ and simulated XRD pattern for (high temperature H) monoclinic phase (*P*2/*c*) according to the NPD structure parameters. The arrows show special peak positions belonging to H-phase. (b) Structure evolution from $P2_1cn$ (cell parameters: *a* = 7.9841(5) Å, *b* = 11.8192(8) Å, *c* = 5.7393(4) Å) to *Pnna* (cell parameters: *a*=11.895(2) Å; *b*=11.6721(3) Å; *c*=7.9714(5) Å) involving cell doubling.

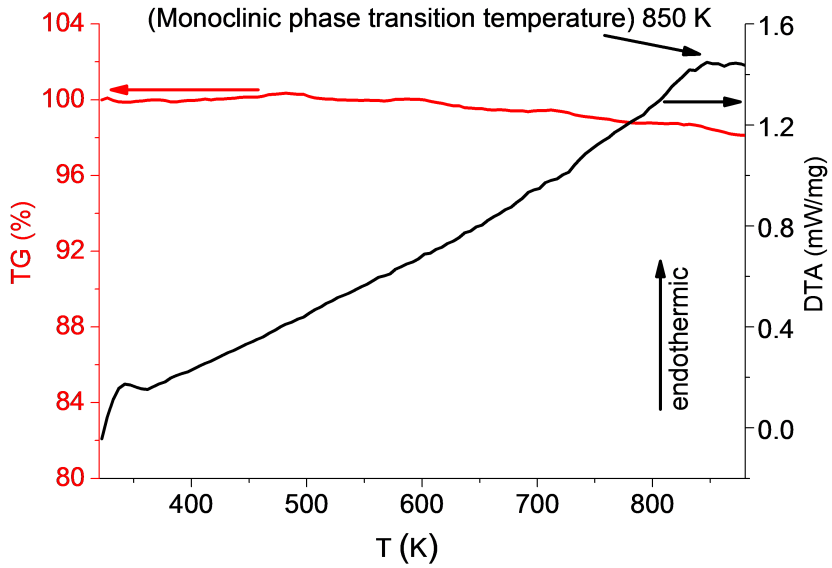

Figure S11. TG and DTA curves of $KBiFe_2O_5$. No evidence of decomposition was observed from the TG curve. The irreversible structural transition of monoclinic phase can be distinctly observed from DTA curve.

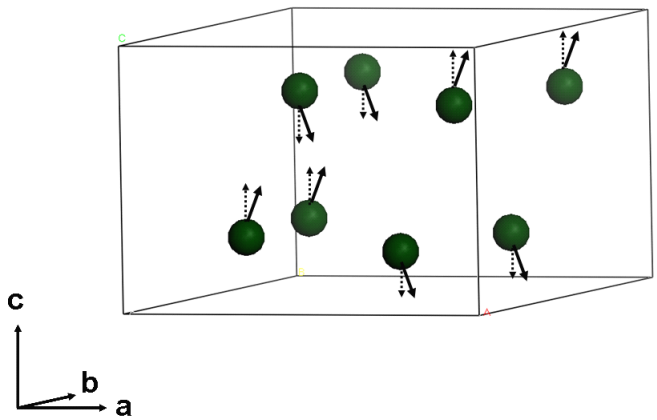

Figure S12. Schematic illustration of spin-canting behavior in $KBiFe_2O_5$. Dotted arrows indicate the G-type spin structure and solid arrows indicate the spin orientation induced by magnetic field.

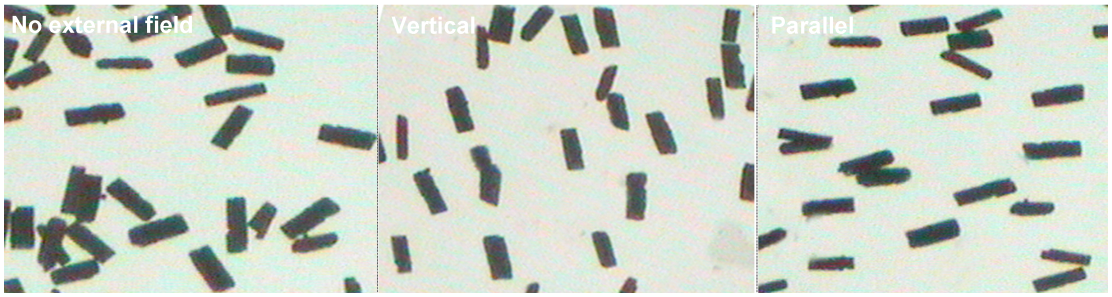

Figure S13. Optical images of crystals responding to the external magnetic field in different directions.

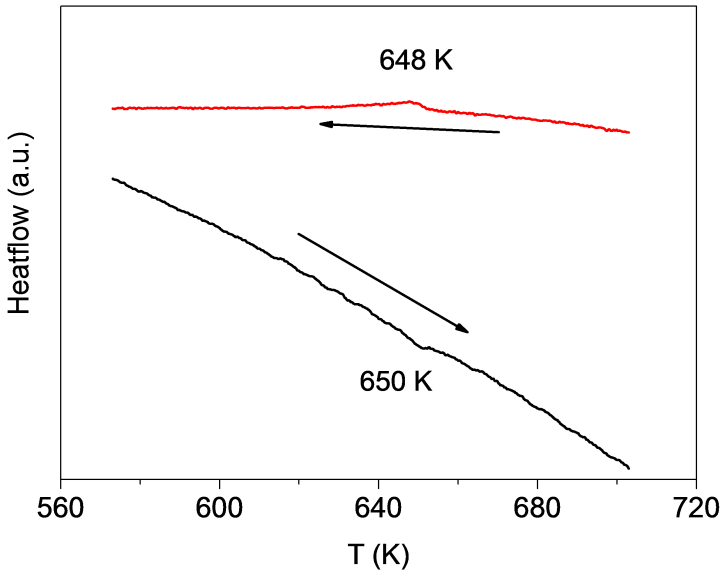

Figure S14. DSC traces during heating and cooling showing a broad transition at 650K which can be identified as the onset of the domination of the AFE phase.

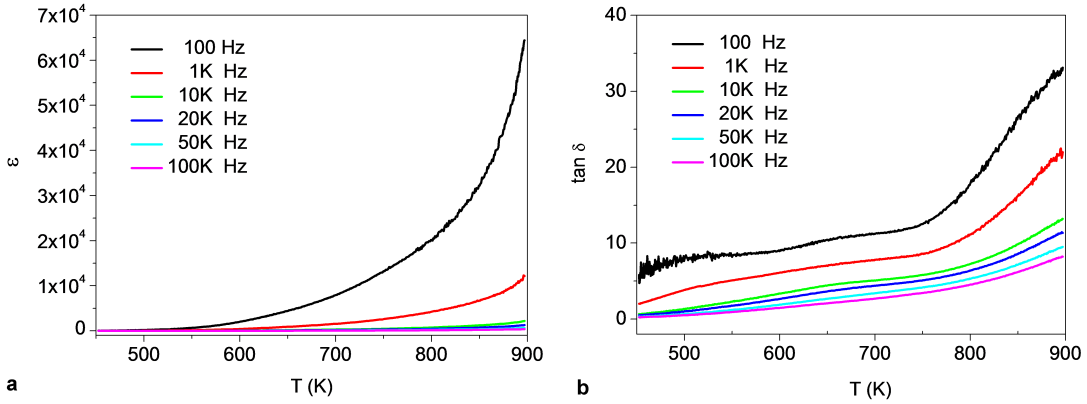

Figure S15. (a) Dielectric constant and (b) tangent loss of monoclinic phase (*P*2/*c*) as a function of temperature measured at $10^{2\text{-}5}$ Hz, using amplitude of 1 V.

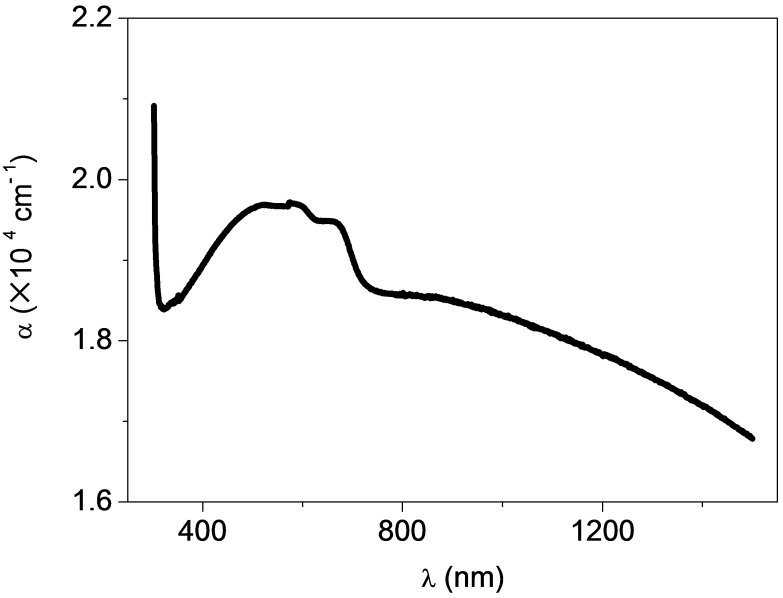

Figure S16. The light absorption coefficient (α) of $KBiFe_2O_5$.

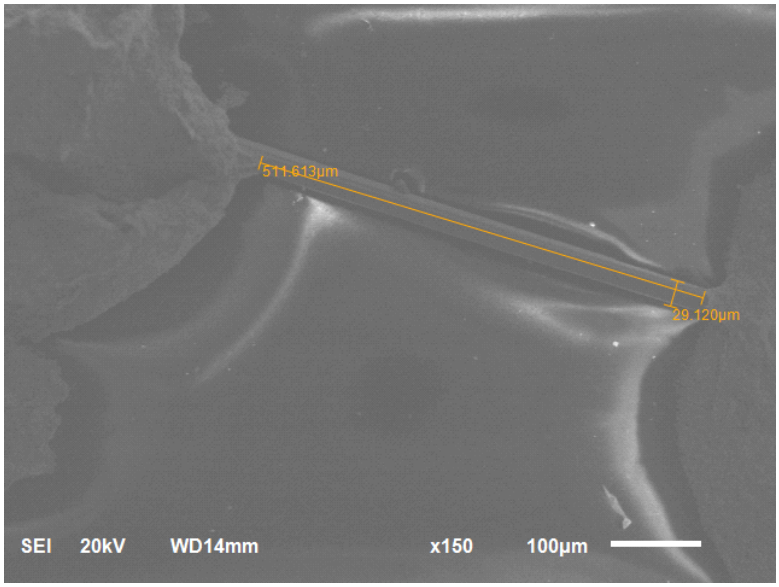

Figure S17. SEM image of the measurement setup of $KBiFe_2O_5$.

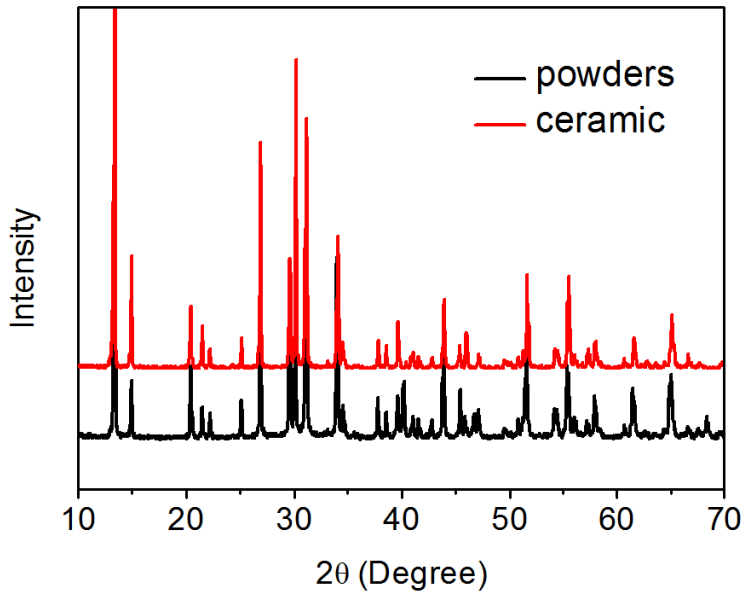

Figure S18. The XRD comparison between the $KBiFe_2O_5$ powders and ceramic.